Letters

An Operation Mode Selection Method of Dual-Side Bridge Converters for Efficiency Optimization in Inductive Power Transfer

Shuxin Chen, *Student Member, IEEE*, Yang Chen, *Student Member, IEEE*, Hongchang Li, *Member, IEEE*, Nguyen Anh Dung, *Member, IEEE*, Ruikun Mai, *Senior Member, IEEE*, Yi Tang, *Senior Member, IEEE*, and Jih-Sheng Lai, *Life Fellow, IEEE*

***Abstract*—In inductive power transfer systems, impedance matching is critical in obtaining high efficiency. However, since the load impedance is subject to variations in most applications, especially wireless charging, maintaining impedance matching is a challenge. One valid solution is to maintain the equivalent load impedance at the optimal value against load variations by controlling a load-side power converter. Nonetheless, the system overall cost, size, and complexity can be increased. In this article, based on a proper selection between full-bridge and half-bridge modes of the inverter and rectifier, an operation mode selection method is proposed that can achieve semi-impedance-matching with large load variations. In general, with the proposed method, high overall efficiency can be obtained while neither additional power converters nor complicated control is required. A 1-kW prototype has been developed and the experimental results have verified the proposed method.**

***Index Terms*—Bridge converter, efficiency optimization, inductive power transfer, wireless power transfer.**

I. Introduction

INDUCTIVE power transfer (IPT) allows wireless power transfer between source and load, and has superior performance over traditional wired systems, such as safety and convenience, especially in charging applications [1]–[5]. Researchers have pointed out that, for a given pair of IPT coils, there exists an optimal loading impedance that maximize the IPT system efficiency [6]–[8]. Hence, impedance matching is a crucial factor in developing a high-efficiency IPT system. Through a proper design of the IPT system parameters, impedance matching can be achieved at one operating point. Nonetheless, in practical applications, especially device charging, both coupling and loading conditions can vary, which inevitably diverges the system from the impedance matching status and leads to lower system efficiency. To overcome the issue, a power converter can be applied to adaptively change the equivalent load impedance to achieve impedance matching, which is also known as maximum efficiency point tracking (MEPT) [7]. In general, through the cooperation of a transmitter-side and a receiver-side power converter, output power regulation and efficiency optimization can be achieved simultaneously in MEPT methods. For example, in [9]–[11], the MEPT control significantly improves the IPT system efficiency with a desired output within a large load range. An ON–OFF keying modulation scheme is also proposed in [12] that only uses one power converter to achieve MEPT and output regulation. As most MEPT methods tend to have a relatively slow response, a novel MEPT method is later developed in [13] that achieves a fast response. Nonetheless, despite the obvious advantages, MEPT methods have several drawbacks. For instance, the use of multiple controllable power converters, real-time communication, and cooperative control can increase system cost, size, and complexity. Moreover, although MEPT can optimize the IPT efficiency, the system overall efficiency is not necessarily improved due to the additional loss on the power converters. Therefore, it may not always be cost effective to implement MEPT.

In this letter, an operation mode selection (OMS) method is proposed that can maintain high efficiency against load variations. Compared to conventional MEPT [7], [10] methods, the most appealing advantage of OMS is that there are no additional power converters or complicated control, as the principle of OMS is to properly select the inverter/rectifier from full-bridge (FB) mode and half-bridge (HB) mode for semi-impedance-matching (semi-IM). The term "semi" indicates that OMS only closely matches the equivalent impedance to the optimal value, which is, although not as accurate as in MEPT, enough to provide a satisfying efficiency enhancement. Compared to [14] which used rectifier mode control [15] for efficiency improvement, one main difference is that the system output basically

Manuscript received January 19, 2020; revised February 15, 2020; accepted February 25, 2020. Date of publication March 9, 2020; date of current version June 23, 2020. This work was part of the research program of Maritime Research Between Singapore (Singapore Maritime Institute) and Norway (Research Council of Norway) under Project SMI-2019-MA-02, which was supported by the Singapore Maritime Institute. *(Corresponding author: Hongchang Li.)*

Shuxin Chen and Yi Tang are with the School of Electrical and Electronic Engineering, Nanyang Technological University, Singapore 639798, Singapore (e-mail: chen1095@e.ntu.edu.sg; yitang@ntu.edu.sg).

Yang Chen and Ruikun Mai are with the School of Electrical Engineering, Southwest Jiaotong University, Chengdu 611756, China (e-mail: yang.chen92@foxmail.com; mairk@swjtu.edu.cn).

Hongchang Li is with the School of Electrical Engineering, Xinjiang University, Urumqi 830046, China (e-mail: hongchangli@xju.edu.cn).

Nguyen Anh Dung and Jih-Sheng Lai are with the Future Energy Electronics Center, Virginia Polytechnic Institute and State University, Blacksburg, VA 24061 USA (e-mail: adnguyen@vt.edu; laijs@vt.edu).

Color versions of one or more of the figures in this article are available online at http://ieeexplore.ieee.org.

Digital Object Identifier 10.1109/TPEL.2020.2979769

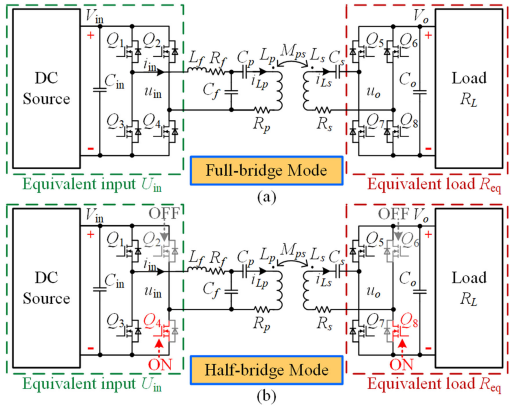

Fig. 1. System diagram of LCC-S IPT in (a) FB mode and (b) HB mode.

remains unchanged in OMS. Generally, OMS and most existing efficiency-improving methods offer different advantages, and the most suitable method is to be selected based on design requirements and preferences.

In principle, OMS is applicable to IPT systems with dual-side active full-bridge converters. Meanwhile, OMS is most suitable for constant-voltage (CV)-type compensation topologies but is less suitable for constant-current (CC) and other types of compensation topologies. The main advantage of OMS is the efficiency improvement, especially for the light-load conditions, with low hardware and software requirements. In this letter, the OMS method is presented by using an inductor–capacitor–capacitor-series (LCC-S) compensated IPT system as an example. The experimental results with a 1-kW prototype have verified that the proposed method can significantly enhance system efficiency with almost no additional cost.

II. Principle of the Proposed Method

Fig. 1(a) presents a typical FB LCC-S IPT system, where the dc source block and the FB inverter form an equivalent IPT input $U_{\rm in}$ while the load R_L block and the FB rectifier form an equivalent IPT load $R_{\rm eq}$. Q_1-Q_4/Q_5-Q_8 are the switching devices of the FB inverter/rectifier, respectively. In Fig. 1(b), by always keeping Q_2/Q_6 OFF and Q_4/Q_8 ON, the original FB inverter/rectifier behaves as an HB inverter/rectifier and the IPT system is changed into HB mode. Therefore, it is possible to change the bridge converters between FB mode and HB mode without additional devices. Apparently, there are two direct consequences of the mode change (MC): 1) $U_{\rm in}$ is changed by inverter FB/HB modes, and 2) $R_{\rm eq}$ is changed by rectifier FB/HB modes.

As has been proven [6]–[8], the IPT efficiency is maximized in impedance matching condition, i.e., $R_{\rm eq}$ equals an optimal value $R_{\rm eq\text{-}opt}$. Therefore, the main principle of OMS is to properly change the rectifier FB/HB mode to make $R_{\rm eq}$ closer to $R_{\rm eq\text{-}opt}$, which leads to higher IPT efficiency. Meanwhile, OMS selects an appropriate inverter FB/HB mode to change $U_{\rm in}$, which helps to maintain the system output. The following section shows the detailed analysis in LCC-S IPT about how semi-IM can be achieved through OMS and the corresponding impact to the system output and efficiency.

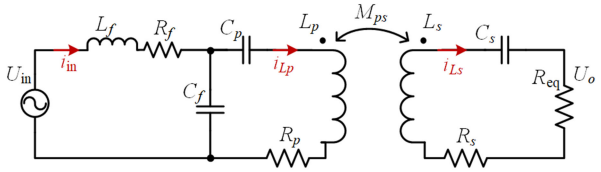

Fig. 2. Simplified LCC-S IPT system.

III. Theoretical Analysis

By applying fundamental harmonic approximation (FHA), the LCC-S IPT in Fig. 1 can be simplified, as in Fig. 2, where $U_{\rm in}$ and U_o are, respectively, the rms values of equivalent sinusoidal input and output voltages at the fundamental frequency f_s. The loading $R_{\rm eq}$ represents the equivalent impedance of the load-side power converters and the system loading R_L. L_f, L_p, and L_s correspondingly represent the inductances of the filter inductor, primary-side coil, and the secondary-side coil. Similarly, C_f, C_p, and C_s symbolize the compensation capacitors while R_f, R_p, and R_s stand for the equivalent series resistances (ESRs) of each inductor (the device turn-ON resistance and capacitor ESR can be included as well), respectively. Besides, M_{ps} is the coil mutual inductance. The resonator parameters satisfy

$$2\pi f_s = \omega_s = \frac{1}{\sqrt{L_f C_f}} = \frac{1}{\sqrt{(L_p - L_f)\, C_p}} = \frac{1}{\sqrt{L_s C_s}} \quad (1)$$

where ω_s is the system angular switching frequency. With (1), according to [16] and assuming lossless, there are

$$\begin{cases} I_{Lp} \approx \frac{U_{\rm in}}{\omega_s L_f} \\ U_o \approx U_{\rm in} \frac{M_{ps}}{L_f} \\ I_{Ls} \approx I_{\rm in} \frac{L_f}{M_{ps}} \end{cases} \quad (2)$$

where I_{in}, I_{Lp}, and I_{Ls} are the rms values of i_{in}, i_{Lp}, and i_{Ls}, respectively. In general, (2) provides a good approximation while greatly simplifying the system analysis.

A. Load Voltage Expression

From (2) and Fig. 1, assuming that the inverter and rectifier electrical gains are, respectively, $G_{\rm inv} = U_{\rm in}/V_{\rm in}$ and $G_{\rm rec} = V_o/U_o$, there is

$$V_o = V_{\rm in} G_{\rm inv} \frac{M_{ps}}{L_f} G_{\rm rec}. \quad (3)$$

Clearly, (3) indicates that the load voltage is independent of the system load R_L as both $G_{\rm inv}$ and $G_{\rm rec}$ are not related to R_L. Thus, LCC-S IPT has a CV output [4], [16]. For charging applications, a battery management converter can be connected between the CV output and the batteries [17], which will not be discussed in this article.

B. IPT Efficiency Expression

The IPT efficiency η can be written as

$$\eta = \frac{I_{Ls}^2 R_{\rm eq}}{I_{\rm in}^2 R_f + I_{Lp}^2 (R_p) + I_{Ls}^2 (R_{\rm eq} + R_s)}. \quad (4)$$

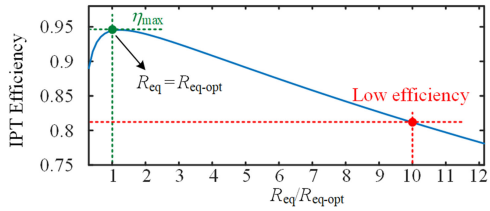

Fig. 3. IPT system efficiency versus normalized R_{eq}.

TABLE I
SYSTEM CHARACTERISTICS UNDER OMS

Mode	G_{inv}	G_{rec}	R_{eq}	V_o
FB	$\frac{2\sqrt{2}}{\pi}$	$\frac{\pi}{2\sqrt{2}}$	$\frac{8R_L}{\pi^2}$	$V_{in}\frac{M_{ps}}{L_f}$
HB	$\frac{\sqrt{2}}{\pi}$	$\frac{\pi}{\sqrt{2}}$	$\frac{2R_L}{\pi^2}$	$V_{in}\frac{M_{ps}}{L_f}$

Knowing that I_{Lp} and I_{Ls} hold the relationship

$$I_{Lp}\omega_s M_{ps} = I_{Ls}(R_s + R_{eq}) \tag{5}$$

by combining (2) and (5), (4) can be derived as

$$\eta = \frac{1}{1 + 2\frac{R_s R_p}{\omega_s^2 M_{ps}^2} + \frac{R_p}{\omega_s^2 M_{ps}^2}R_{eq} + \left(R_s + \frac{{R_s}^2 R_p}{\omega_s^2 M_{ps}^2} + \frac{M_{ps}^2}{{L_f}^2}R_f\right)\frac{1}{R_{eq}}}. \tag{6}$$

Hence, there exists an optimal R_{eq}, denoted as $R_{eq\text{-}opt}$, that maximizes (6)

$$R_{eq-opt} = \sqrt{\omega_s^2 M_{ps}^2 \frac{R_s}{R_p} + R_s^2 + \omega_s^2 M_{ps}^2 \frac{M_{ps}^2}{L_f^2}\frac{R_f}{R_p}}. \tag{7}$$

Based on (6) and (7), Fig. 3 is drawn that describes the relationship between η and R_{eq}. When R_{eq} is greatly different from R_{eq-opt}, e.g., $R_{eq} = 10R_{eq-opt}$, the IPT efficiency will be much lower than the optimal value.

Therefore, to have high nominal efficiency, LCC-S IPT systems are usually designed to be impedance matching under the nominal situation, i.e., nominal air gap and load. Nonetheless, when the system operating point varies, especially when a large load change occurs, which is common in charging applications, the impedance matching status will be lost, and the system efficiency will be thereby reduced. As discussed before, the proposed OMS method can effectively solve the efficiency reduction issue for the light-load conditions.

C. Operation Mode Selection

For LCC-S, the OMS method requires both the inverter and rectifier to change between FB mode and HB mode. The ideal electrical gains of conventional inverter and rectifier G_{inv} and G_{rec} under both FB and HB modes have been well discussed in [9] and [10], and are listed in Table I. Combined with (3), the respective R_{eq} and V_o under the two modes for LCC-S IPT are also given in Table I.

From Table I, the LCC-S system in FB and HB modes have the same output voltage but different R_{eq}. Thus, when the IPT system deviates from the optimal point due to load change, by applying OMS, V_o is unchanged while R_{eq} can be again adjusted to be close to $R_{eq\text{-}opt}$, which will improve the system efficiency.

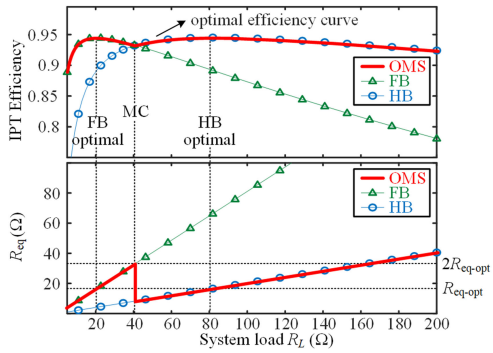

Fig. 4. Theoretical efficiency under FB mode, HB mode, and OMS.

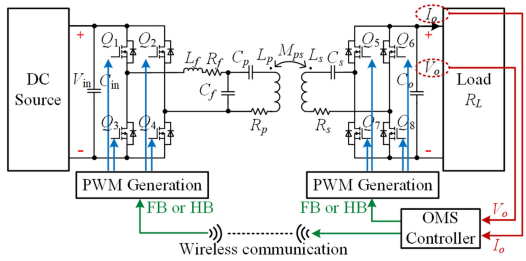

Fig. 5. One implementation of OMS.

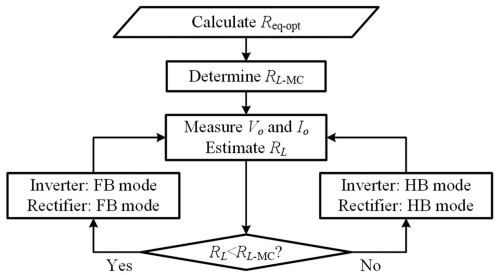

Fig. 6. Flowchart of the OMS controller for LCC-S.

Fig. 4 demonstrates one example of the following.

1) The FB and HB modes have different optimal R_L that lead to $R_{eq} = R_{eq-opt}$ and the highest efficiency.
2) The efficiency of either FB or HB mode quickly drops with a large load variation.
3) OMS helps to maintain semi-IM ($R_{eq} \approx R_{eq-opt}$), which combines the optimal section of the FB and HB efficiency curves and achieves high overall efficiency.
4) The MC point R_L (40 Ω) is the geometric mean of the corresponding R_L at the FB and HB optimal points (20 and 80 Ω), which is discussed in the next section.

Hence, the proposed OMS method is capable of improving system efficiency without affecting the system output or introducing additional hardware.

IV. IMPLEMENTATION

Fig. 5 provides one possible implementation of the proposed OMS method, where the flowchart of the OMS controller is described in Fig. 6. In principle, OMS requires the measurement of V_o and I_o to evaluate the load R_L. By comparing the estimated

R_L with the MC point $R_{L-\mathrm{MC}}$, the OMS controller determines whether the inverter and rectifier should be in FB or HB mode. Subsequently, the OMS signals are sent to the pulse width modulation (PWM) generation of the inverter and rectifier to realize MC.

A. MC Point R_{L-MC}

The ideal MC point $R_{L-\mathrm{MC}}$ is the load value for the system efficiency under FB and HB modes to be identical, which can be obtained from (6), (7), and Table I. As the corresponding R_L for optimal efficiency under FB and HB modes are $R_{L-\mathrm{opt-FB}} = R_{\mathrm{eq-opt}}\pi^2/8$ and $R_{L-\mathrm{opt-HB}} = R_{\mathrm{eq-opt}}\pi^2/2$, $R_{L-\mathrm{MC}}$ is the central point (geometric mean) of $R_{L\text{-opt-FB}}$ and $R_{L\text{-opt-HB}}$, i.e.,

$$R_{L-\mathrm{MC}} = \sqrt{R_{L-\mathrm{opt-FB}} R_{L-\mathrm{opt-HB}}} = \frac{\pi^2}{4} R_{\mathrm{eq-opt}}. \quad (8)$$

The experimental results provided in Section V have verified (8). Meanwhile, if necessary, adding hysteresis to $R_{L-\mathrm{MC}}$ is one effective way against potential instability, which is not shown in Fig. 6.

B. Measurement

V_o and I_o are measured to estimate R_L. Since OMS is mainly for efficiency optimization, a fast response to load changes is not critical, and hence, the bandwidths of measurement circuits need not be high.

C. Communication

In Fig. 5, to acknowledge the inverter for MC, wireless communication is used. Since OMS is only activated at the MC point, frequent information exchanges between the primary and secondary sides are not required by OMS, which avoids constantly occupying the communication link. Moreover, in the worst case that the inverter did not apply MC due to unknown reasons while the rectifier applied MC, the output voltage would vary, and the rectifier should return to the original mode to restore the output.

D. Variations of M_{ps}

In real applications, M_{ps} is usually variable due to the coil misalignment. From (7) and (8), since $R_{L-\mathrm{MC}}$ is related to M_{ps}, the real-time monitoring of M_{ps} is required to obtain $R_{L-\mathrm{MC}}$. However, to avoid adding the monitoring circuit, it is also possible to use $R_{L-\mathrm{MC}}$ in the nominal M_{ps} for all misaligned conditions, which is less optimal but still offers satisfying performance. Relative experiments and explanations could be found in Section V-C.

E. Mode Selection for Different Topologies

In the example LCC-S IPT system, OMS requires both the inverter and rectifier to change from FB mode to HB mode. However, this may not apply to other compensation topologies, and the study in Section III should be repeated to determine the optimal mode combination. The following facts generally hold.

1) Most CV topologies have a similar output expression to (3). Hence, the design in Fig. 6 is suitable, i.e., both the inverter and rectifier are to be changed from FB to HB modes (or reversely) in OMS to achieve semi-IM without affecting the output.
2) For most CC topologies, to achieve semi-IM without affecting the output, when the rectifier changes from FB to HB, the inverter has to change from HB to FB and vice-versa. This combination is less common, as most IPT systems are designed to have both bridge converters under the same mode. Additional regulating power converters are to be considered [17].

Consequently, although OMS is theoretically applicable to different topologies, OMS is most suitable for CV topologies and is less suitable for CC and other topologies.

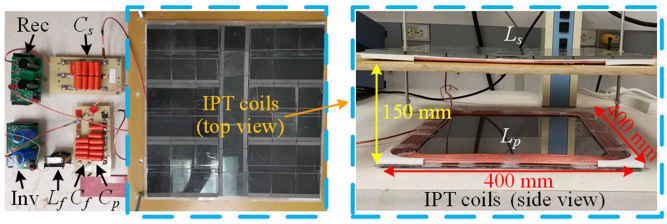

Fig. 7. Photos of the prototype.

TABLE II
PARAMETERS OF THE PROTOTYPE

Symbol	Description	Value
L_p	primary-side coil inductance	148.2 μH
L_s	secondary-side coil inductance	150.4μH
L_f	filter inductor inductance	84 μH
M_{ps}	mutual inductance	28.4μH
C_p	primary-side compensation capacitance	46.7 nF
C_s	secondary-side compensation capacitance	23.0 nF
C_f	filter capacitance	40.9 nF
f_s	switching frequency	85 kHz

V. Experimental Verification

A. System Introduction

Following Fig. 1, a 1-kW LCC-S IPT prototype, as shown in Fig. 7, is developed to verify the proposed method with most parameters given in Table II. The system input voltage is 380 V dc while the load voltage is around 130 V under the nominal air gap of 150 mm. Similar to conventional designs, the IPT system efficiency is optimized around full-load condition with the FB inverter and rectifier.

B. Experimental Results and Comparison

Fig. 8(a) shows the efficiency curves under FB, HB, and OMS against R_L. For the conventional FB design, the system efficiency gradually dropped from 94.5% to around 76.8% as R_L increased from 16 to 200 Ω (load power from around 1 kW to 85 W), mainly due to the loss of impedance matching. The highest efficiency 94.5% occurred at $R_L \approx 18$ Ω. In contrast, under HB mode, the system efficiency was found to be the highest when $R_L \approx 75$ Ω, but the power dissipation was severe under heavy-load conditions, e.g., the system loss at $R_L = 20$ Ω is about 71.1 W ($P_o \approx 680$ W, $\eta \approx 89.5$ %). With OMS, the system efficiency was well maintained at a relatively high

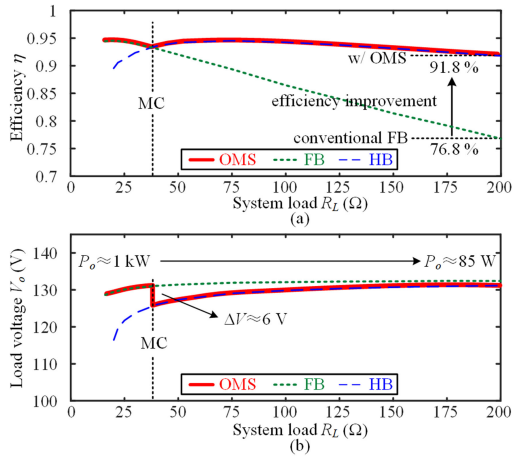

Fig. 8. Experimental results under FB mode, HB mode, and OMS: (a) efficiency, and (b) load voltage.

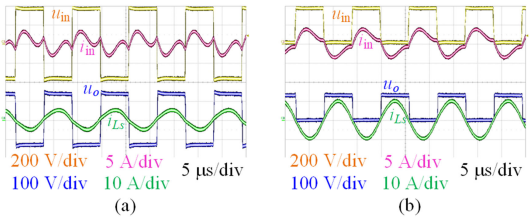

Fig. 9. System steady-state waveforms around MC point: (a) FB mode, and (b) HB mode.

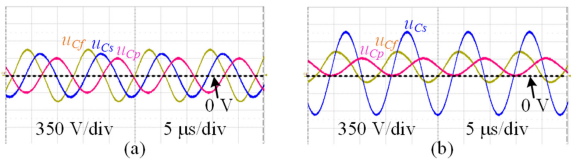

Fig. 10. Steady-state voltages of resonant capacitors around MC point: (a) FB mode, and (b) HB mode.

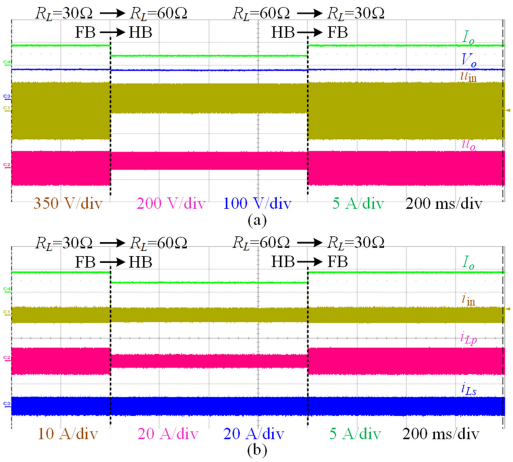

Fig. 11. System dynamic waveforms of OMS with load step changes: (a) voltage, and (b) current.

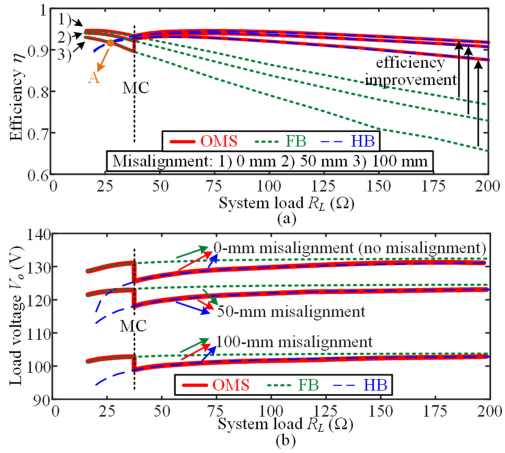

Fig. 12. Experimental results under FB mode, HB mode, and OMS with various misalignments: (a) efficiency, and (b) load voltage.

level (91.8%–94.5%) within the whole load range, which clearly proves the effectiveness of the proposed method. Compared to the conventional dual-side FB design, the efficiency around the full-load conditions was not improved, since the system loading was already around the optimal point. However, OMS took effect after the MC point, and especially, at the lightest load condition, the system efficiency was improved from 76.8% to 91.8% by OMS. In addition, Fig. 8(b) shows the load voltage curve, where OMS caused a small voltage drop at the MC point, which is due to component tolerance and parasitic.

Besides, the system steady-state waveforms under FB mode and HB mode are given in Fig. 9 as well as the capacitor voltages in Fig. 10, where dc biases can be observed under the HB mode. As the resonant currents and voltages at the MC point are lower than the ones at the full-load point, the increased currents and voltages due to the MC can still be within designed limits. The corresponding dynamic waveforms of OMS are shown in Fig. 11, where load step changes were deliberately applied (which were represented by the I_o step changes in the waveforms) to trigger OMS from FB mode to HB mode as well as from HB mode to FB mode, with $R_{L-\mathrm{MC}} \approx 37\ \Omega$. The observed system transients during the mode transition were not severe, as both the inverter and rectifier well performed the MC. Moreover, for charging applications that changes the load power slowly, OMS could be designed to be only triggered once at the MC point for the whole charging process, which will further simplify the measurement and control of OMS.

C. Misalignments

The effect of OMS under misaligned conditions has also been examined. The main consequence of misalignment is the change of M_{ps}. Horizontal misalignments of 50 and 100 mm were applied to the coils in Fig. 7, which decreases M_{ps} from around 28.4 to 26.9 and 22.5 μH, respectively. The experiments in Fig. 8 were repeated with the two misalignments, and the results are provided in Fig. 12.

In Fig. 12(a), with OMS, the system efficiency was obviously improved as compared to the conventional FB design. In Fig. 12(b), with misalignments, the voltage changes caused by OMS were also small. However, the nominal voltage values

varied based on misalignments, which complied with (3) and was a system characteristic of LCC-S compensation that was not caused or deteriorated by OMS.

Moreover, according to Section IV, the MC points should be different when M_{ps} is different. For instance, in Fig. 12(a), under the 100-mm misalignment, activating OMS at the highlighted point A could lead to higher efficiency than at the used MC point. However, to monitor M_{ps}, additional measurement circuits or estimation algorithms could be required. This experiment deliberately used the same $R_{L-\mathrm{MC}}$ calculated from the nominal condition (no misalignment) for all situations, and the results indicated that the efficiency-improving effect was still satisfying. Thus, the real-time tracking of M_{ps} is beneficial to OMS, but is not a must.

Therefore, for applications where misalignments exist, OMS can be applied to improve system efficiency. However, the output variation due to misalignments is not caused by and cannot be solved by OMS. Typically, using a power converter for output regulation [17] or adopting advance coil designs [18] are possible approaches to maintain the output. However, such a regulating power converter is not related to the core principle of OMS and would not be discussed.

D. Discussion

In Fig. 8(a), with OMS, the system efficiency experiences fluctuations, e.g., the MC point efficiency is lower than the surrounding points. The reason is that OMS only achieves semi-IM and cannot always maximize the IPT efficiency as in typical MEPT methods [10], [11], [13]. Nonetheless, the most outstanding advantage of OMS is the obvious efficiency enhancement with low hardware and control requirements. In general, MEPT and OMS have different benefits, and should be selected based on practical application requirements.

VI. Conclusion

This letter introduces an efficiency-improving method for IPT called OMS. In principle, OMS is based on impedance matching and is implemented through properly selecting the operating modes of the inverter and rectifier. Compared to conventional impedance matching methods such as MEPT, the unique advantage of the proposed method is that basically no additional hardware or complicated control algorithm is required. A 1-kW LCC-S IPT prototype is used to evaluate the proposed method. In the experiment, with OMS, the system efficiency was maintained between 92%–95% from 85 W to 1 kW, while the system efficiency would be 77%–95% if without OMS. Moreover, OMS can also effectively improve system efficiency under misaligned conditions, but advanced coil designs or additional circuits are required to maintain system output against misalignments, which is another topic that is unrelated to OMS.

References

[1] S. Y. R. Hui, "Past, present and future trends of non-radiative wireless power transfer," *CPSS Trans. Power Electron. Appl.*, vol. 1, no. 1, pp. 83–91, Dec. 2016.

[2] J. Feng, Q. Li, F. C. Lee, and M. Fu, "Transmitter coils design for free-positioning omnidirectional wireless power transfer system," *IEEE Trans. Ind. Inform.*, vol. 15, no. 8, pp. 4656–4664, Aug. 2019.

[3] S. Li and C. C. Mi, "Wireless power transfer for electric vehicle applications," *IEEE J. Emerg. Sel. Topics Power Electron.*, vol. 3, no. 1, pp. 4–17, Mar. 2015.

[4] Y. Chen *et al.*, "Variable-parameter T-circuit-based IPT system charging battery with constant current or constant voltage output," *IEEE Trans. Power Electron.*, vol. 35, no. 2, pp. 1672–1684, Feb. 2020.

[5] X. Qu, H. Chu, S.-C. Wong, and C. K. Tse, "An IPT battery charger with near unity power factor and load-independent constant output combating design constraints of input voltage and transformer parameters," *IEEE Trans. Power Electron.*, vol. 34, no. 8, pp. 7719–7727, Aug. 2019.

[6] Z. Zhang, H. Pang, A. Georgiadis, and C. Cecati, "Wireless power transfer—An overview," *IEEE Trans. Ind. Electron.*, vol. 66, no. 2, pp. 1044–1058, Feb. 2019.

[7] H. Li, J. Li, K. Wang, W. Chen, and X. Yang, "A maximum efficiency point tracking control scheme for wireless power transfer systems using magnetic resonant coupling," *IEEE Trans. Power Electron.*, vol. 30, no. 7, pp. 3998–4008, Jul. 2015.

[8] Y. Zhang, T. Kan, Z. Yan, and C. C. Mi, "Frequency and voltage tuning of series–series compensated wireless power transfer system to sustain rated power under various conditions," *IEEE J. Emerg. Sel. Topics Power Electron.*, vol. 7, no. 2, pp. 1311–1317, Jun. 2019.

[9] R. Mai, Y. Liu, Y. Li, P. Yue, G. Cao, and Z. He, "An active-rectifier-based maximum efficiency tracking method using an additional measurement coil for wireless power transfer," *IEEE Trans. Power Electron.*, vol. 33, no. 1, pp. 716–728, Jan. 2018.

[10] H. C. Li, J. Y. Fang, S. X. Chen, K. P. Wang, and Y. Tang, "Pulse density modulation for maximum efficiency point tracking of wireless power transfer systems," *IEEE Trans. Power Electron.*, vol. 33, no. 6, pp. 5492–5501, Jun. 2018.

[11] X. Dai, X. F. Li, Y. L. Li, and A. G. P. Hu, "Maximum efficiency tracking for wireless power transfer systems with dynamic coupling coefficient estimation," *IEEE Trans. Power Electron.*, vol. 33, no. 6, pp. 5005–5015, Jun. 2018.

[12] W. Zhong and S. Y. R. Hui, "Maximum energy efficiency operation of series-series resonant wireless power transfer systems using on-off keying modulation," *IEEE Trans. Power Electron.*, vol. 33, no. 4, pp. 3595–3603, Apr. 2018.

[13] Z. C. Huang, S. C. Wong, and C. K. Tse, "Control design for optimizing efficiency in inductive power transfer systems," *IEEE Trans. Power Electron.*, vol. 33, no. 5, pp. 4523–4534, May 2018.

[14] M. Zimmer, J. Heinrich, and N. Parspour, "Design of a 3 kW primary power supply unit for inductive charging systems optimized for the compatibility to receiving units with 20 kW rated power," in *Proc. 4th Int. Elect. Drives Prod. Conf.*, 2014, pp. 1–5.

[15] M. Fan, L. Shi, Z. Yin, L. Jiang, and F. Zhang, "Improved pulse density modulation for semi-bridgeless active rectifier in inductive power transfer system," *IEEE Trans. Power Electron.*, vol. 34, no. 6, pp. 5893–5902, Jun. 2019.

[16] Y. S. Yao, Y. J. Wang, X. S. Liu, and D. G. Xu, "Analysis, design, and optimization of LC/S compensation topology with excellent load-independent voltage output for inductive power transfer," *IEEE Trans. Transp. Electrific.*, vol. 4, no. 3, pp. 767–777, Sep. 2018.

[17] M. Kim, D.-M. Joo, and B. K. Lee, "Design and control of inductive power transfer system for electric vehicles considering wide variation of output voltage and coupling coefficient," *IEEE Trans. Power Electron.*, vol. 34, no. 2, pp. 1197–1208, Feb. 2019.

[18] Y. Chen *et al.*, "A hybrid inductive power transfer system with misalignment tolerance using quadruple-D quadrature pads," *IEEE Trans. Power Electron.*, vol. 35, no. 6, pp. 6039–6049, Jun. 2020.